

REPRODUCIBILITY OF THE ORIGINAL PAGE IS POOR.

77.11.3 4-496.2

(NASA-CR-115750) SYSTEM DESIGN AND	N72-28468
PERFORMANCE OF EARTH/LUNAR HORIZON SENSOR	
BEC PROJECT 3744 Final Report F. Schwarz,	
et al (Barnes Engineering Co.) 21 Oct.	Unclas
1966 62 p	CSCL 20F G3/14 36642



Faint, illegible text at the bottom of the page, possibly bleed-through from the reverse side.

NAS 9-1462
495

BARNES ENGINEERING COMPANY

30 Commerce Road

Stamford, Connecticut

Technical Report
TR 3744-11A

Final Report

System Design and Performance
of Earth/Lunar Horizon Sensor
BEC Project 3744

Prepared By:

F. Schwarz
T. Falk
G. Falbel
P. Spangenberg

APPROVED BY

Frank Schwarz, for
R. W. Astheimer
Technical Director
Defense and Space Division

October 21, 1966

TABLE OF CONTENTS

	P.
1. Introduction	1-1
2. Description of Horizon Sensor System Design	1-1
2.1 Detector	2-3
2.2 Electronic Processing	2-4
2.3 Offset Radiation Source Operation	2-5
2.4 Optical System	2-7
3. Expected Performance and Error Analysis	3-1
3.1 Accuracy Considerations	3-1
3.2 Measured Sensitivity and Expected Performance of Earth/Lunar Horizon Sensor	3-11
4. Measurements Made to date	4-1
4.1 Detector and input Circuit Drift	4-1
4.2 Detector Responsivity	4-2
4.3 Measurement of Gain and Frequency Response	4-2
4.4 Noise Measurements	4-4
4.5 Response Time Measurement	4-4
4.6 Offset Heat Source Operating Characteristics	4-5
4.7 Power Consumption	4-6
4.8 Physical Characteristics of the Horizon Sensor	4-6

TABLE OF CONTENTS (Continued)

	P.
5. Reliability Estimate for Thermopile Horizon Edge Tracker (Based on a three headed system)	5-1
5.1 Summary	5-1
5.2 Reliability Estimate	5-1
5.3 Failure Rate	5-2
5.3.1 Standard MIL Spec Parts	5-2
5.3.2 "Hi-Rel" Parts	5-3
6. Present Status of Horizon Sensor System and Evaluation of Problem Areas	6-1
6.1 Modulator Drive Signal Pickup	6-1
6.2 Offset Heat Source	6-2
6.3 Evacuation of Optical Barrel	6-4
7. Present Status of Program and Conclusions	7-1

LIST OF ILLUSTRATIONS

- Fig. 1 Cross Section of Thermopile Horizon Edge Tracker
- Fig. 2 Block Diagram of One Head Thermopile Horizon Edge Tracker
- Fig. 3a Lens Objective
- 3b Aspheric Sag for Lens Objective
- 3c Lens, Field Flattening, Drawing
- 3d Lens, Field Flattening, Spectral Characteristics
- Fig. 4 Horizon Profiles 14-35 Micron Range
- Fig. 5 Horizon Profiles Showing Field of View Indentation
- Fig. 6 Spectral Transmission of Sensor Optics
- Fig. 7 Time Response for Transient Attitude Change
- Fig. 8 Photograph of Thermopile Edge Tracker
- Table 5-1 Reliability Parts Breakdown page 5-5
- Table 5-2 Reliability Parts Breakdown (Cont.) page 5-6

1. Introduction

This report is being prepared in conformance with the contract requirements at a time prior to complete checkout and testing of the Earth/Lunar horizon sensor. The report will therefore concentrate on a detailed description of the design and operating features of the horizon sensor. We will not repeat discussions of features of the system which have already been presented in previous reports such as the Phase IB Design Study Report.

At the end of this discussion we will present that portion of the evaluation test data which has been completed. Final test data will be presented at the time the instrument is delivered, after completion of performance tests. That data may then be appended to this Engineering Report in order to define the performance of the sensor more completely.

2. Description of Horizon Sensor System Design

An infrared horizon sensor system has been designed which is capable of searching over a wide field for the edges of a planet and, upon locating such edges, stations itself in a position which provides signals which identify the local vertical to the planet. In this fixed attitude it requires no continuous mechanical movement and operates with a minimum utilization of power. The system is thus capable of providing a high degree of accuracy when used for local vertical determination in orbits around the earth the moon or other planets. It also has a high reliability figure. Among the

many other features of the system is a capability for operation, with high accuracy, over a wide range of altitudes including synchronous altitude, avoidance of the common cloud lock-on problem, elimination of high-speed moving parts and the ability to function even under high vibration such as during powered flight.

The present program is limited to development of a single optical head capable of tracking only one horizon edge - three or four heads or two paired telescopes would normally be used for pitch and roll determination. The evaluation of the performance of the single head configuration becomes somewhat restricted since one head is not capable of providing a local vertical output but simply measures an arbitrary angle. There is also no provision for possible switchover to an alternate telescope in the event of the appearance of the sun in the field of view. The discussion which follows will be concerned principally with the basic design of a single sensor.

It will be recalled that the particular concept chosen for this edge tracking horizon sensor evolved from the system trade-off study conducted early in the program and some experience at Barnes Engineering Company with a system similar to that now used. The reasons for this choice and the parametric study of various horizon sensor system concepts were the subjects of the several Engineering Reports submitted in the earlier phases of this program.

2.1 Detector

The detector used in this horizon sensor is a Barnes vacuum-deposited thermopile using bismuth-tellurium thermocouple junctions. These thermopiles, as well as another type developed by Barnes using bismuth-antimony junctions, have been developed and tested over a 3-year period and have shown themselves to be extremely rugged and reliable thermal detectors over ambient temperature ranges of -200°C to $+100^{\circ}\text{C}$. In this case, two thermopile detectors are mounted on the base plate of the optical telescope. The areas covered by the thermopile active junctions subtend fields of view of 1.15° in elevation by 8° in azimuth and have dimensions of 1.27 mm in elevation by 8 mm in azimuth. These thermopiles are made up of 48 thermocouple junction pairs.

In air the specific responsivity of these thermopiles has been measured to be 0.67 volts/watt/cm². It will be noted in Figure 1 that the thermopile detectors are mounted on the pivoted assembly along with integrated circuit preamps and MOSFET modulators. Thus, to minimize electrical pickup problems, high level signals are fed out through the pivoted assembly shafts using torsionally twisting wires. The success and reliability of this type of signal feedout was first experimentally proven by torsionally twisting a set of 10 No. 38 wires through a ± 45 angle for 50,000 cycles over ambient temperature ranges of -35°F to $+150^{\circ}\text{F}$. No degradation in the wires was noted during or after this test.

2.2 Electronic Processing

The electronic processing configuration of the sensor head is shown in Figure 2. It will be noted that no mechanical chopping or scanning is required to produce the horizon tracking signal. Rather, the d.c. microvolt-level output of the thermopile produced by the received horizon irradiance is sampled by a Metal Oxide Semiconductor Field Effect Transistor (MOSFET) low-level switch. (This thermopile signal sampling technique has been under development at Barnes for over a 2-year period. Development tests have demonstrated that a commutation noise and offset level of less than ± 1 microvolt can be obtained over a temperature range of -55°C to $+85^{\circ}\text{C}$. As of this date only preliminary test data was obtained on the present horizon sensor program in which a different detector (20 element Bismuth Tellurium thermopile) was used as the test sample.

The sampled thermopile signal is amplified and demodulated and serves to control the pulse width of a variable period monostable multivibrator, which, in turn, feeds variable width power pulses to a brushless d.c. torquer. The variable pulse width drive results in a great economy in power as well as tending to relieve the mechanical "stiction" produced in the bearings of the pivoted member. The fixed downward drive is also applied in a pulsed mode. At tracking equilibrium, the two opposite motor drive pulses will be in phase, so that minimum power will be consumed.

Separate search and track modes are not required for this sensor, since the downward drive applied to the torquer provides a search function and tracking is automatically achieved when the lower field of view intersects the horizon. If for some reason the horizon is not acquired on the first downward pass when the sensor is turned on, the downward drive on the servo moves the pivoted member to the bottom limit stop, at which point a magnetically actuated reed switch is engaged. This sets a flip-flop, thus in turn producing an upward bias signal which drives the servo to its top limit switch, which in turn resets the flip-flop so that the downward drive horizon search action begins again, until a horizon is acquired. Servo rate stabilization is accomplished with the use of a brushless d.c. tachometer whose output serves to control the amount of fixed downward drive. This signal processing approach results in a uni-polar gain-loop concept which greatly reduces the number of electronic parts in the system.

2.3 Offset Radiation Source Operation

The offset radiation source shown in Figures 1 and 2 is used to minimize the offset voltage present at the thermopile detectors when the sensor views cold space. This thermopile offset voltage is a function of the sensor ambient temperature. If the offset radiation source were not used, a relatively large negative d.c. term would be added to the A and B detector outputs and the effect on the sensor errors of any detector responsivity mismatch would be

greatly accentuated. The offset radiation source serves to radiatively "heat up" the thermopile active junctions so that the A and B thermopiles produce essentially zero microvolts when they view cold space.

The offset radiation source is closed-loop controlled by the summed outputs of detectors A and B. This control loop compares the detector outputs to ground potential and applies power to the offset radiation source until any negative output of the detectors is removed. Since in normal system operation the A detector always views space and the major portion of B also views space, the space offset terms of both thermopiles are automatically reduced to essentially zero by the offset radiation source. It should be emphasized that this is true even if there is a responsivity mismatch between the A and B detectors, because a responsivity mismatch is analogous to a difference in detector absorptivity. Therefore, it can be shown that a thermopile detector having a low absorptivity (i.e., low emissivity) will have a low space offset term; but by the same token, it will also accept less IR radiant energy from the offset radiation source. This powerful self-compensating effect of the offset radiation source was demonstrated in the Barnes-developed LPHS sensor, in which an array of 90 thermopiles was irradiated with an offset radiation source with the result that the space offset term in the thermopile was reduced to one microvolt when the sensor viewed a liquid nitrogen background. To date we have

made measurements with the telescope of our sensor viewing dry ice with the result that the offset heat source reduced imbalances at the input to approximately $1/\mu\text{Volt}$.

2.4 Optical System

The Earth/Lunar Horizon Sensor optical system employs a 2.5" Diameter f/1 aspheric lens made of Silicon as the objective. A second element of the system a field flattener silicon lens is located immediately in front of the detector and also serves as the substrate for a 14 micron cut on interference filter (see Fig. 3a-d lens design). This interference filter, coupled with the normal fall-off in transmission of Silicon at about 35μ , produces an optical pass band of 14-35 microns and encompasses the $\text{CO}_2\text{-H}_2\text{O}$ atmospheric absorption bands which are considered to be satisfactory regions of operation in earth-orbiting missions. The same spectral region is quite favorable for operation on lunar missions. No change in detector or optics is thus required for any of the missions envisaged. Fig. 3b represents measured lens contours as they approach the ideal aspheric shape during fabrication.

3. Expected Performance and Error Analysis

3.1 Accuracy Considerations

There are five main sources of error in the measurement of horizon declination angle for each sensor head:

e_1 - error due to earth anomalies and horizon radiance variations.

e_2 - error due to inaccuracy of angular readout transducer.

e_3 - error produced by noise and drift.

e_4 - error produced by a gain change in signal amplification loop.

e_5 - error produced by alignment inaccuracies.

e_1 - This error comes about due to IR radiance and spatial variation of the effective earth horizon due to season, geography, or cloud cover. To evaluate this error for the thermopile edge tracking horizon sensor, we have used the results of a computer study conducted by Wark, et al*, to obtain the horizon profile radiance curves ($N_{\lambda} \eta$) shown in Figure 4. Each point on these horizon profiles is

$$\int_{14\mu}^{35\mu} N_{\lambda} \eta_{\lambda} d\lambda$$

*Wark, D.Q., Alishouse, J., and Yamamoto, G. "Calculation of the Earth's Spectral Radiance for Large Zenith Angles," Meteorological Satellite Laboratory Report No. 21, October 1963.

and was computed using the measured spectral transmission (η) of a typical silicon optical system (shown in Figure 6) and the values of N_λ for each altitude.

The horizon profiles in Figure 4 are plotted as a function of altitude above and below the true horizon. The abscissa can be converted to angular changes in the line of sight to the horizon as a function of orbit altitude. For example, at a 100-mile orbit altitude, 10 km \approx 0.39° shift in the line of sight to the horizon; at 200 miles, 10 km \approx 0.23° shift, etc.

Using this relationship, we can find the edge tracking points for the two worst case horizon profiles (curves B and C) which are plotted in Figure 5. (Note: Curve D was also considered but does not apply at low altitudes due to geographical considerations.) Let us set the downward drive in the edge tracker servo loop so that a 0.2 horizon indentation will produce a servo null for the coldest, sharp (i.e., high altitude orbit) horizon edge. At a 100-mile altitude, the field of view edge half-power point indents into the horizon profile to the +20 km point on the B curve, and a servo null will occur when:

$$\int_0^{\infty} (N_{\Delta\lambda\eta})_B R_{(FOV)} dh = \int_0^{\infty} (N_{\Delta\lambda\eta})_C R_{(FOV)} dh \quad (1)$$

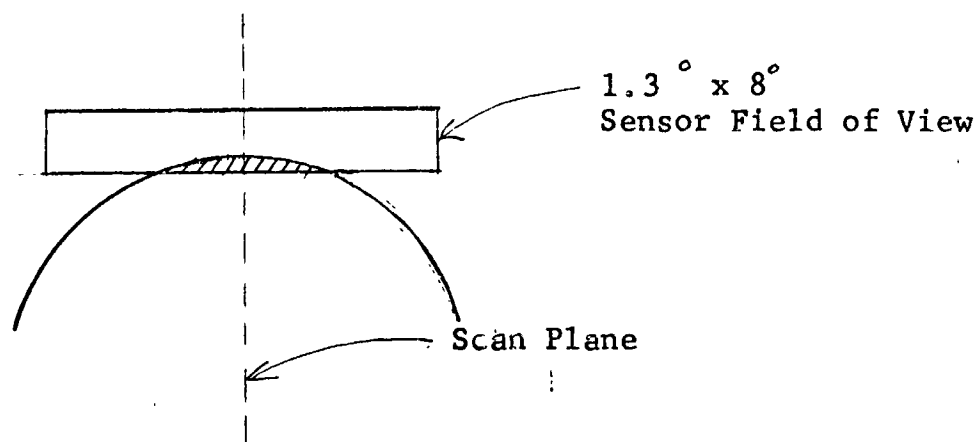
where

$R_{(FOV)}$ = spatial response of the horizon sensor field of view edge. This is defined by the aberrations of the optics which will produce a blur circle of 0.1

Of course, the spatial projection of the 0.1° FOV edge blur will depend on the orbit altitude. The edge blur relationship to the horizon profile shown in Figure 5 is applicable to 100 and 200 mile altitudes. The two integrals in equation (1) were obtained by a planimeter measurement of the applicable cross-hatched areas in Figure 5, and the two horizon edge positions which satisfied equation (1) were obtained by an iterative process. As can be seen in Figure 5, the distance between the two field of view positions for the two worst case horizon radiance profiles (B and C) is only 4 km which, at a 100-mile orbit altitude, is equivalent to $\pm 0.08^\circ$ from a nominal declination angle. At a 200-mile altitude, 4.5 km is equivalent to $\pm 0.063^\circ$.

At very high altitudes (10,000 to above 22,000 miles), the calculation of the e_1 error is complicated due to the earth curvature. At these altitudes, the generated signal is proportional to the area of the "cusp" defined by the intersection of

the sensor's field of view with the circular earth horizon as shown below:



In each case, a servo null is obtained when the solid angle defined by the cusp (Ω_c) is such that:

$$G N_{\Delta\lambda} \Omega_c = K$$

where

G = optical and electronic gain of the sensor (nominally constant)

$N_{\Delta\lambda}$ = earth spectral radiance (variable)

K = a constant equivalent to the fixed downward drive on the servo

It can be seen from the above drawing that Ω_c changes non-linearly with linear angular increments of the earth in the scan plane at altitudes where the chord of the cusp is less than 8° .

Let us set the fixed downward drive on the sensor so that, at the servo null, $\Omega_c = 1.6(\text{deg})^2$ for the coldest horizon edge.

(This is equivalent to a 0.2° horizon indentation angle at low altitudes, so that $\Omega_c = 0.2^\circ \times 8^\circ$. (The 0.2° value is chosen to eliminate the effect of the 0.1° field of view edge blur produced by optical aberrations.)

Under the above constraints, an analysis has shown that a 1.8:1 radiance ratio between opposite earth limbs will produce an e_1 error of $\pm 0.08^\circ$ at 22,000 miles, and $\pm 0.12^\circ$ at 40,000 miles.

However, it should be pointed out that for high altitude, low eccentricity orbits the field of view edge can be readily shaped with a field mask to conform to the earth curvature at a nominal mid-point altitude. For this case, Ω_c would take the shape of a sector of an annulus, would vary linearly with earth increment angles, and would have a maximum horizon indentation angular dimension of 0.2 for the coldest horizon edge ($N_{\Delta\lambda C}$). Therefore, if curved field edges are used, it can be shown that, for $N_{\Delta\lambda B}/N_{\Delta\lambda C} = 1.8$, $e_1 = 0.2^\circ/1.8 = 0.11 = \pm 0.055^\circ$ for any altitude from 6000 to 100,000 miles.

It can therefore be concluded that for orbits with high eccentricities, where conformal field shaping cannot be used, $e_1 < 0.1^\circ$ for altitudes between 100 and 20,000 miles, increasing to $\pm 0.1^\circ$ below altitudes of 100 miles and to $\pm 0.12^\circ$ at 40,000 miles. For near-circular, high-altitude orbits, where conformal field shaping can be used, a $\pm 0.05^\circ$ value can be assigned to e_1 .

Since our design goals specify a maximum altitude of 300 n. mi. conformal field shaping will not be required.

e₂ - This error results from the inaccuracy of the shaft angular transducer used on the sensor. While either analog or digital encoders could be used, the digital type providing a higher accuracy capability at the expense of greater cost and a higher parts count, the contract specified an analog readout. The angular transducer shown in Figure 1 is a synchronous resolver made by Reeves Instruments. This type was chosen over others made by Kearfott, Daystrom, etc. because of its higher accuracy. This type of readout provides a $\pm 0.05^\circ$ readout accuracy if adequate precaution has been taken in designing the reference AC source to be free from Frequency and amplitude variations over the entire operating temperature range. A great deal of effort was put into the design of such a stable source of AC power. By the use of larger transducers, readout accuracies to ± 1 minute of arc are obtainable. Digital angular encoders of the photoelectric type (Baldwin Electronics Company) or the multi-speed resolver type (Inductosyn) can provide readout accuracies better than ± 0.5 arc-minute. Due to the construction of the sensor head, an interchangeable angular readout capability is provided; and depending upon the accuracy required for a given mission, a suitable readout can be used.

Since the e_1 error will be the predominating one in this sensor, an angular transducer providing $\pm 0.05^\circ$ such as was chosen is considered to be adequate, therefore we will use a value of $e_2 = \pm 0.05^\circ$ in our error budget estimation.

e_3 - This error results from noise and drift generated in the thermopile detectors and low-level switching circuitry.

Preliminary experimental results show a noise and drift level of approximately ± 1 microvolt related to the detector signal level including the thermopile, the MOSFET modulator and a small amount of pickup of the modulator drive signal which has not as yet been eliminated.

In order to refer this ± 1 microvolt noise and drift voltage to the equivalent angular error, we must calculate the thermopile detector scale factor (Δv_t) for a 0.1° angular shift of the horizon edge.

$$\Delta v_t = R' \frac{A_o}{A_d} N_{\Delta\lambda} \eta \Delta\Omega$$

where

R' = thermopile detector specific responsivity = 1.3 volts/watt-cm²

A_o = aperture area = 31.6 cm²

A_d = detector area = 1.27 x 8.5mm = 0.11 cm²

$N_{\Delta\lambda} \eta$ = lowest horizon spectral radiance x optical transmission
at field of view edge = 1.5×10^{-4} watts/cm²-ster
(see Figure 5)

3 - 8

$\Delta\Omega$ = change in horizon solid angle for 0.1 angular shift
= 0.1 x 8 = 2.5 x 10⁻⁴ steradians

$$\therefore \Delta v_t = 1.3 \times \frac{31.6}{0.1} \times 1.5 \times 10^{-4} \times 2.5 \times 10^{-4}$$

$$\Delta v_t = 14 \text{ microvolts}/0.1^\circ$$

Therefore, a +1 microvolt drive referred to the detector level will be equivalent to 0.1°/14 or +0.007°, so that

$$e_3 = \underline{+0.007^\circ}.$$

The above calculation assumes the use of the 14 to 35 micron spectral region.

e₄ - This error comes about due to a change in the responsivity of the "B" thermopile, or a change in the gain of the signal amplification loop. The effect of such a change would be that the amount of "upward" drive for a given horizon indentation angle would be changed, so that a tracking null would be reached at a different horizon declination angle. If we conservatively allow a +5% variation in this loop gain, this is equivalent to an uncompensated earth radiance change of +5%. By using the techniques discussed for e₁, the value of e₄ = +0.015°.

e₅ - This error is produced by misalignment of the sensor head relative to the horizon simulator and involves the angular accuracy of the simulated horizon obtainable with the horizon simulator. In this regard, the horizon declination angle for each sensor head would be read out for each sensor head by mounting the head on a precision rotary table and comparing the sensor head angular transducer output with the horizon declination angle set on the precision rotary table. Alignment of the sensor heads would be achieved by zeroing the angular transducer for a known horizon declination angle and relating this zero setting to an autocollimation surface on the sensor.

If we assume a rotary table accuracy of $\pm 0.01^\circ$ and an autocollimation accuracy of $\pm 0.01^\circ$, $e_5 = \pm 0.014^\circ$.

Error Summary - The 3 σ error for each head of this sensor system (e_{total}) is:

$$e_{total} = \sqrt{(e_1)^2 + (e_2)^2 + (e_3)^2 + (e_4)^2 + (e_5)^2}$$

Without radiance compensation, for the worst case at 100 mile altitude:

$$e_{total} = \sqrt{(\pm 0.08^\circ)^2 + (\pm 0.05^\circ)^2 + (\pm 0.007^\circ)^2 + (\pm 0.015^\circ)^2 + (\pm 0.014^\circ)^2}$$

$$e_{total} = \pm 0.097^\circ \text{ at 100 miles}$$

At 200 mile altitude:

$e_{\text{total}} = \pm 0.083^\circ$, asymptotic to $\pm 0.078^\circ$ with conformal field shaping at high altitudes.

The above errors are equal to 0.707 of the total system 3σ error at null for a three-headed system, where the heads are situated -45° , $+45^\circ$, and $+135^\circ$ in azimuth relative to the vehicle pitch axis, and:

$$\Delta\text{Pitch} = (+45^\circ \text{ head}) - (-45^\circ \text{ head})$$

$$\Delta\text{Roll} = (+45^\circ \text{ head}) - (+135^\circ \text{ head})$$

This is true, since:

$$e_{\text{system}} = \frac{e_{\text{total}}}{\sin 45^\circ} = 1.414 e_{\text{total}}$$

where

e_{total} is increased by $1/\sin 45^\circ$, because a 1° Δpitch or Δroll produces a change in horizon declination angle in each head of 1° ($\sin 45^\circ$), and errors in each head have the corresponding converse effect.

It can therefore be concluded that, with the exception of earth oblateness errors, this horizon sensor system without radiance compensation can provide a 3σ null accuracy range against the real earth horizon of $\pm 0.078^\circ$ to $\pm 0.14^\circ$, depending upon altitude, number of heads, and orbit eccentricity.

3.2 Measured Sensitivity and Expected Performance of Earth/Lunar Horizon Sensor

The foregoing error analysis is based on infrared radiance levels as encountered in earth orbit missions. With the measured sensor parameters we can also predict the performance of the sensor in a lunar orbit over the prescribed altitudes of 50 to 150 n.m.

To justify both the values of error cited in the foregoing discussion and that which follows we will compute the instrument sensitivity for the expected radiance levels encountered on the moon. The voltage developed by the detector if its field of view were fully on a lunar surface of 100 K is given by

$$V_D = \frac{\int \Delta N_{\Delta\lambda} R'_V \eta}{f^2} \quad (\text{see TR 3744 IB, Phase 1B Design Report})$$

The radiance in the spectral interval 14-40 μ for a 100°K black body surface, $N_{\Delta\lambda} @ 100^\circ K = 9.5 \times 10^{-5}$ Watts/cm² ster

The f_{no} of the optical system is $f_{no} = 1$

The specific responsivity of the detector,

$$R'_V = 1.3 \text{ Volts/Watt/cm}^2 \text{ (in vacuum)}$$

η = efficiency of the optical elements = .35

$$V_D = \frac{\int}{4} \frac{9.5 \times 10^{-5} \times 1.3 \times .35}{(1)^2} = .34 \mu V$$

for full field coverage.

For a planet indentation of 0.1° the signal developed becomes

$$V_D / 0.1^\circ = 34 \mu V \times \frac{0.1^\circ}{1.15^\circ} \approx 3 \text{ mVolts} / 0.1^\circ$$

It should be noted that this is a conservative figure since it assumes that the entire region irradiating a $0.1^\circ \times 8^\circ$ detector subtense is at a temperature of 100°K . In general, crater edges which may at times have this low a temperature will occupy a small portion of this field of view, the balance being at considerably higher temperatures.

4. Measurements made to date

A number of tests were conducted in various phases of the construction of the earth/lunar horizon sensor. Most of these were intended as means for testing the functioning of various portions of the system. As was stated earlier the final measurements will be presented after all data has been taken and upon delivery of the horizon sensor.

In this section we will report the information gathered at various stages in the construction of the sensor. This includes: measurement of drift of the detector and input circuitry, detector responsivity measurement, gain and frequency response measurements, noise measurements, response time tests, transfer function determination offset heat source operating characteristics, measurements of power consumption and mechanical and physical characteristics of the sensor.

4.1 Detector and input circuit drift

Prior to assembly of the sensor telescope a Bismuth Tellurium thermopile (not the one now being used) was connected to the front-end electronics including the MOSFET modulator and was placed in an environmental chamber and cycled in temperature from -30 C to +60 C. The demodulated preamplifier output was recorded on a Sanborn chart recorder. A small stable DC signal was periodically injected at the detector for calibration and as a check on system gain.

The drift of the input circuitry which resulted, both variations with temperature and repeatability at any specific temperature was just slightly under one microvolt, referred to the input.

4.2 Detector Responsivity

The responsivity of the two detectors used was measured prior to their installation using a Barnes black-body source and chopper. The two units measured .7Volts/watt/cm and .67Volts/watt/cm² in air.

Experience indicates that when they are mounted in the telescope and the compartment is evacuated the responsivity will double so that a final responsivity of 1.4V/watt/cm is expected. In this process the time constant will degrade from a value of 100 m sec. The resistance of the detectors was measured to be about 67,000 ohms.

4.3 Measurement of gain and frequency response

The combined gain of the preamplifier — postamplifier — demodulator — low pass filter channel is

$$4.2 \text{ m V d.c. output} / \begin{matrix} 1 \text{ V peak-peak} \\ \text{a.c. input} \end{matrix}$$

This is the signal that modulates the duty cycle of the voltage wave and thus the electrical power applied to the torquer motor. The scale factor of this process is

$$\frac{67 \text{ m A incremental stator current}}{100 \text{ m V incremental low pass filter output}}$$

In terms of locked motor torque of the torquer motor this becomes

$$\frac{1.0 \text{ ounce-inch incremental torque}}{100 \text{ m A incremental stator current}}$$

or the total electro-mechanical gain

$$\frac{4.2}{1} \times \frac{67}{100} \times \frac{1.0}{100} =$$

$$\frac{0.0281 \text{ oz. in. incremental torque}}{1 \text{ microvolt peak to peak incremental input}}$$

This indicates that the 3.0 microvolt signal corresponding to an incremental dip of 0.1 degree of arc into a 100°k moon is sufficient to overcome by a factor of 8 the bearing stiction torque of 0.01 oz. in. The safety margin is actually greater than that because of the very small dither due to the residual 25 cps and 1000 cps ripple.

The bandwidth of the preamplifier - postamplifier combination is 1.2 cps - 710 cps. The commutation rate is 30 cps. The overall electronic bandwidth is determined by the low pass filter following the demodulator. It is set at d.c. - 1 cps.

4.4 Noise Measurements

The equivalent input noise voltage in the preamplifier — postamplifier bandwidth (710 cps) has been measured as 1.6 μ V. rms. At the output of the low pass filter (1 cps bandwidth) this becomes

$$\frac{1.6}{\sqrt{710}} = 0.06\mu\text{V rms}$$

This shows that the instrument is drift (0.5-1.0 microvolt) rather than noise limited.

4.5 Response Time Measurement

The oscillogram of Fig. 7 indicates a response time of about 200 milliseconds for the edge tracker. In these tests the rotating barrel was held fixed in positions dipped into and away from the simulated horizon and then suddenly released. It is seen that the response time for both initial positions is essentially the same, but the character of the transient is different, with a swell overshoot in the case of the field of view originally dipped into the horizon. The reason for this is the difference in the average system loop-gain (averaged over the time of the transient) controlling the two types of motion.

At the time this measurement was made the present readout system was not yet available and the ripple riding over the traces is that of the rectified output of an induction potentiometer excited with 400 cps.

4.6 Offset Heat Source Operating Characteristics

While testing the effectiveness of the offset heat source it was found that the 600 m W maximum power originally assigned to the heater was not sufficient and that almost 1000 m W power was needed. The increase in power has been achieved by changing the driving mode from half wave to full wave.

The drive characteristics have been changed in one further respect. The original linear mode of operation has been changed to bang-bang by introduction of a Schmitt trigger in the drive control. This was done in order to speed up the response of the offset heat source control loop.

The step common mode signal (common to both A and B thermopiles) when suddenly facing space (simulated by a block of dry ice) with the thermopile mounting plate at 25°C

is about 550 micro volt. This common mode signal is reduced by the action of the offset heat source to about 5% of its original value.

4.7 Power Consumption

The power consumption of the tracking head has increased from the original estimate of 1.2 watts to about 1.6 watts due to the increase in offset heat source power consumption. (See 4.6)

4.8 Physical Characteristics of the Horizon Sensor

The dimensional measurements of the sensor can be seen from the mechanical drawing, Fig. 1 and the photograph, Fig. 8.

The weight of significant individual components and the total weight of one separate optical head is given in the table below:

<u>Item</u>	<u>Weight (lbs.)</u>
End Bells	0.22
Electronic Mounting Rings	0.27
Angular Readout Mount	0.13
Angular Readout	0.25
Torquer and Tachometer Mounts	0.32
Torquer and Tachometer	0.8
Silicon Lens and Filter	0.11
Pivoted Assembly including Detectors, Bearings, and Shafts	0.2
Cylindrical Housing	0.28
PC boards with Electronic Components	0.5
Miscellaneous Cabling and Connector	0.1
	<u>3.20 lbs.</u>

Some of the weights of individual components itemized above are estimated values. The final total, however, less power supplies was weighed as 3.25 lbs. The weight of the sensor can be further reduced (at increased cost) if beryllium or magnesium are used for the housing and structure.

5. Reliability Estimate for Thermopile Horizon Edge Tracker
 (Based on a three headed system)

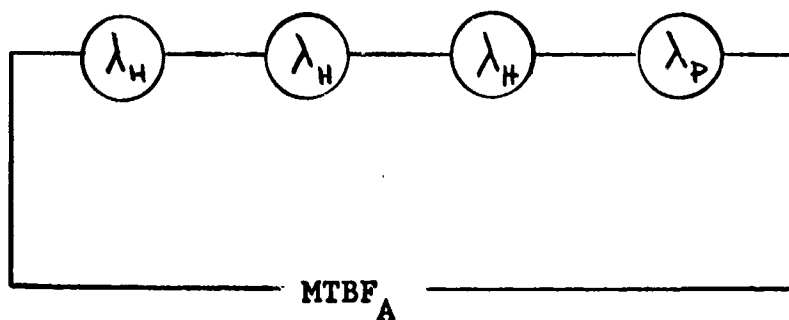
5.1 Summary

A preliminary reliability estimate, based on a "worst case" parts type/parts count analysis at +60°C, results in an estimated MTBF of 197,600 hours using "Hi-Rel" parts and 15,020 hours using standard MIL spec parts, for a system consisting of three heads and a power supply.

5.2 Reliability Estimate

A reliability model for the basic system is shown below. The calculations for MTBF utilize the failure rates as outlined in Tables 4-1 and 4-2.

Reliability Model



H = failure rate
of head

P = failure rate
of power supply

$$MTBF_A = \frac{1}{3\lambda_H + \lambda_P} = \frac{1}{(3 \times 20.70) + 4.92 \times 10^{-6}} = \frac{1}{56.62 \times 10^{-6}}$$

= 15,020 hours with standard MIL spec parts

$$MTBF_A = \frac{1}{3\lambda_H + \lambda_P} = \frac{1}{(3 \times 1.611) + 0.228 \times 10^{-6}} = \frac{1}{5.061 \times 10^{-6}}$$

= 197,600 hours with Hi-Rel parts

5.3 Failure Rates

5.3.1 Standard MIL Spec Parts

In preparation of this analysis, base failure rates for all of the part types, except for the silicon photodetector, the integrated circuits, and the thermopiles, have been obtained from MIL-HDBK-217. The silicon detector failure rate was obtained from GE TRA-873-74, "Reliability Analysis Data for Systems and Component Design Engineers," which is distributed by the US Department of Commerce (while no silicon sun protect detector has been incorporated in the present sensor it is assumed that the final system will utilize such a system). The failure rate for the integrated circuits has been conservatively set at five times the failure rate for transistors, as obtained from

MIL-HDBK-217. The thermopiles are manufactured by a vacuum deposition process which results in a unit nearly identical to a thin-film resistor in construction. Therefore, the failure rate for a thin-film resistor, with very little power dissipation or voltage stress, is used for a thermopile.

This analysis is based upon a maximum ambient temperature of +60°C and on a "worst case" assumption that parts are stressed in accordance with the following:

Maximum Stress Ratios

Diodes, Rectifier	20% of rated power
Diodes, Zener	50% of rated power
Transistors	20% of rated power
Resistors, Composition	30% of rated power
Capacitors, Tantalum	35% of rated voltage
Capacitors, Ceramic	40% of rated voltage

5.3.2 "Hi-Rel" Parts

Failure rates for "Hi-Rel" parts have been obtained from TRW Systems Document 80C0.2-124. These failure rates are estimates of what may be obtained in

coming years for high-reliability spacecraft systems, provided that exceptional care is exercised regarding device application, quality assurance, drift screening-aging tests, and other techniques to eliminate "infant mortality" and reduce "random" failures to a minimum.

The synchronous resolver, tachometer, and torquer have been considered as transformers since the rate of rotation of these devices will be negligibly small. Limit switches are treated as relays without coils, the silicon photodetector is treated as a silicon diode, and the thermopiles are considered as comparable to thin-film resistors.

TABLE 5-1 Reliability Parts Breakdown

Function and Component Type	Base Failure Rate (FR x 10 ⁻⁶ /hr)		Qty.	Total Failure Rate (FR x 10 ⁻⁶ /hr)	
	Standard MIL Spec Parts	Hi-Rel Parts		Standard MIL Spec Parts	Hi-Rel Parts
HEAD (three per system)					
Resistor, Composition	0.02	0.002	65	1.30	0.130
Resistor, Wire Wound, Power	0.26	0.002	1	0.26	0.002
Capacitor, Tantalum, Solid	0.18	0.030	17	3.06	0.510
Capacitor, Ceramic	0.01	0.004	7	0.07	0.028
Transistor, Silicon	0.26	0.010	32	8.32	0.320
Diode, Silicon, Rectifier	0.13	0.005	10	1.30	0.050
Integrated Circuit:					
Flip-Flop	1.30	0.050	1	1.30	0.050
Amplifier	1.30	0.050	2	2.60	0.100
Thermopile	0.25	0.002	3	0.75	0.006
Synchronous Resolver	0.32	0.010	1	0.32	0.010
Tachometer	0.32	0.010	1	0.32	0.010
Torquer	0.32	0.010	1	0.32	0.010
Limit Switch	0.20	0.090	2	0.40	0.180
Silicon Photodetector	0.38	0.005	1	0.38	0.005
			H =	20.70	1.611
				x 10 ⁻⁶ /hr	x 10 ⁻⁶ /hr

TABLE 5-2 Reliability Parts Breakdown (Continued)

<u>Function and Component Type</u>	Base Failure Rate (FR x 10 ⁻⁶ /hr)		Qty.	Total Failure Rate (FR x 10 ⁻⁶ /hr)	
	Standard MIL Spec Parts	Hi-Rel Parts		Standard MIL Spec Parts	Hi-Rel Parts
POWER SUPPLY (one per system)					
Resistor, Composition	0.02	0.002	10	0.20	0.020
Capacitor, Tantalum, Solid	0.18	0.030	3	0.54	0.090
Capacitor, Ceramic	0.01	0.004	2	0.02	0.008
Transistor, Silicon	0.26	0.010	4	1.04	0.040
Diode, Silicon, Rectifier	0.13	0.005	8	1.04	0.040
Diode, Silicon, Zener	0.68	0.010	2	1.36	0.020
Transformer, Power	0.32	0.010	1	0.32	0.010
				4.52	0.228
				x 10 ⁻⁶ /hr	x 10 ⁻⁶ /hr

λ_P

5
1
6

6. Present Status of Horizon Sensor System and Evaluation of Problem Areas

The horizon sensor has now been assembled in what should be its final form and is being readied for the final tests to evaluate its performance characteristics.

Several problems were encountered in the course of assembly and checkout of the horizon sensor engineering model and these were reported to NASA/MSC technical personnel in telephone conversations. These should not be considered to be serious and will not prevent the achievement of reliable performance approaching the design goals which had been set. They are of a nature frequently encountered in a development program of a sophisticated instrument of high accuracy and are amenable to correction. Corrective measures are now being taken in these problem areas.

The problems in this category are as follows:

1. Pickup of low level modulator gating signal at preamplifier input
2. Insufficient power in the offset heat source to completely cancel any mismatch in detector responsivities.
3. Insufficient vacuum sealing of optical telescope compartment

6.1 Modulator Drive Signal Pickup

On first turning on the low level modulator input circuit a large amount of in-phase modulation offset signal was observed.

which was not related to signal developed by the detectors. This was found to be caused by pickup of the modulator square wave drive and which leaked into the preamplifier input. The circular circuit board which houses the modulator and preamplifier is located at the base of the optical telescope (near the detectors) and is hand wired. Relocating the leads carrying this reference signals reduced this offset to an acceptable level corresponding to just under one microvolt at the input of the system. The ensuing error is equivalent to about $.05^\circ$ in a lunar mission and less in an earth orbit. A next generation printed circuit board performing the required functions would accomplish a better separation of the reference drive signal from the low level input circuits and reduce the pickup to even smaller values.

6.2 Offset Heat Source

A slight miscalculation of the conductive heat losses to the telescope casing of the offset heat source located at the edge of the optical telescope between the objective lens and the detector base has resulted in a somewhat marginal heating of the detectors. It therefore does not fully restore the loss of heat of the active junctions of the thermopile detectors when they view space (this original design provided for a 600 milliwatt maximum dissipation). As a result a mismatch

of the two detectors (this was measured to be 5%) can result in a small second order error in that an offset signal would appear at the system input due to the differential responsivity even when both detectors viewed the absolute zero space temperature. The offset heat source does indeed turn out to be effective in restoring a good measure of the heat lost by the detectors to space. It thus tends to equalize the temperature of the active junctions with that of the ambient reference junctions thereby making any responsivity mismatch (for a near zero temperature differential) of no consequence. When the optical barrel is evacuated the offset heat source seems to require about 75% more power for creating a zero temperature differential for the two detectors when they are pointed at a block of dry ice. In an unevacuated state, with convection losses added to the conductive and radiative exchange, the offset heat source is less effective yet.

Under normal operating conditions, with the telescope evacuated and with an ambient temperature of 25°C the two detectors develop signals of $550\mu\text{volts}$ and $525\mu\text{volts}$, respectively, when viewing dry ice. The difference, which is modulated and fed to the preamplifier would be $25\mu\text{volts}$ if no offset heat source were used (under these conditions the active junctions are at a temperature about 1°C below that of the reference junctions). With the offset heat

source in operation the active junctions are heated up and under ideal conditions will assume a temperature identical to that of the reference junctions. The offset heat source, as originally designed provided sufficient heat to bring the active junctions to within $.2^{\circ}\text{C}$ of the reference junctions. The remanent offset signal was thus brought down from $25\mu\text{volts}$ to $5\mu\text{volts}$ which was considered to be inadequate. The transient characteristics of the offset heat source control loop was also found to be wanting.

A redesign was undertaken as discussed in Section 4.6, in which offset heat source control electronics was made more efficient through use of a full wave drive circuit and the introduction of a Schmitt Trigger providing maximum drive signal amplitude. As a result of the modifications undertaken the offset heat source is now able to reduce the offset signal to 5% of its original value i.e. $1.25\mu\text{volts}$. This represents less than 0.1° error for a hypothetical 100°K moon. Even assuming a variation in the efficiency or power generated by the offset heat source we will still be within safe limits.

6.3 Evacuation of Optical Barrel

Some difficulty was encountered in achieving a good vacuum with the telescope assembly due to improper seals at the screw-on base of the optical barrel which houses the detectors and

input circuit boards and in the hollow shaft through which the leads are fed from the telescope to the external circuits. O-ring seals proved inadequate in maintaining an adequate vacuum for an extended period of time. Out-gassing takes place at a rate of about 10^{-6} cc/second. A vacuum of 10^{-7} tor has been measured shortly after removal of the evacuation tube but degrades rather rapidly with time. We believe that a sealing compound such as Hysol will permit more adequate vacuum sealing. However we wish to complete all tests and assure ourselves of proper system operation before making the seal final and thereby precluding any possible revisions or readjustments. Design with somewhat tighter tolerances in a next sensor would prevent the difficulties with evacuation presently encountered.

As pointed out earlier, none of the problems cited are expected to hinder the achievement of the performance which has been predicted for the Earth/Lunar Horizon Sensor system.

7. Present Status of Program and Conclusions

At this writing the engineering model Earth/Lunar Horizon Sensor has been completely assembled. The servo loop has been closed and initial tests have been made to establish that the basic system is functioning and is ready for the individual and detailed testing which will be required to fully characterize its performance capabilities.

Certain tests were conducted at various stages of the design and assembly of the system to establish if the individual elements of the system are performing as required and expected. The results of such tests and data have been presented in this and in earlier reports. A procedure has been established for performing the final system checkout tests and instrumentation and simulation equipment is presently being assembled to perform evaluation tests. It is not expected that sufficient time will be available for such tests as vibration, shock, EMI, etc., which are not called for in our contract.

We have reviewed the information presented in the parametric study of horizon sensor systems and which constituted phase IA and IB of this program.* In light of the information presented there, our general experience in the field of horizon sensors and the preliminary observed performance characteristics of the Earth/Lunar Horizon Sensor we are compelled to conclude that the choice which has been made jointly by NASA/MSC and Barnes Engineering Co. and which resulted in the development of the present system concept was the correct one. We believe that this system is capable of performance quite superior to that of other systems developed to date.

The basic features and advantages of the system have already been cited. We wish to repeat only the principal ones:

1. The system uses no continuously moving parts and is capable of long life. In addition it can successfully operate in a vibration environment.

* See earlier engineering reports. Phase IA Study Report, Addendum to Phase IA Report and Phase IB Design Study Report.

2. It achieves a high signal to noise ratio by sensing radiation from the edge of the planet without requiring any scanning (e.g. conical scan over a wide acquisition field) or vibration near the edge of the planet which it tracks. This high signal-to-noise ratio results because only a minimum noise bandwidth is required.
3. It avoids cloud or lunar crater-terminator lock-on problems through use of the field switching technique in which the radiance from the edge of the planet is always compared to a 0°K space reference located far (17.2°) above the horizon.
4. The system is versatile and can achieve a high accuracy when operating in orbits around the earth, the moon or any of the major planets of interest. It should be emphasized that this high accuracy is maintained over a wide range of altitudes including synchronous altitude. No changes in the optics or spectral characteristics of the system are required to achieve this performance.

Since the horizon declination angles are read out through a precision resolver (or digital readout) the sensor's linear range or angular scale factor is independent of the orbit altitude. In addition the sensor can provide a highly accurate readout of the orbital altitude. The inclusion of a tachometer in the sensor design allows the simple generation of vehicle angular rate outputs.

7 - 4

In view of the above discussion we therefore feel that this system can be considered the most advanced development in infrared horizon sensors presently known.

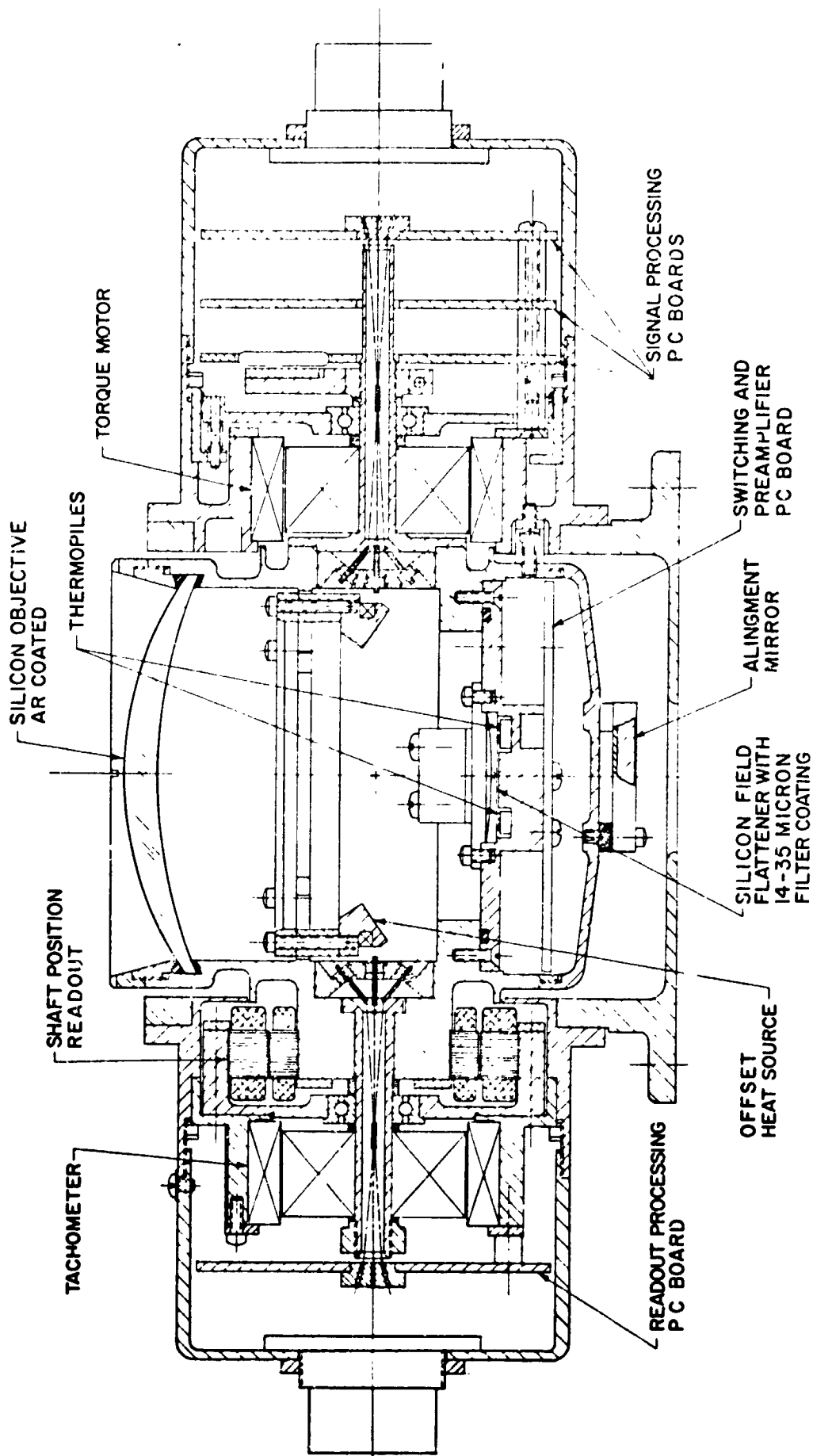
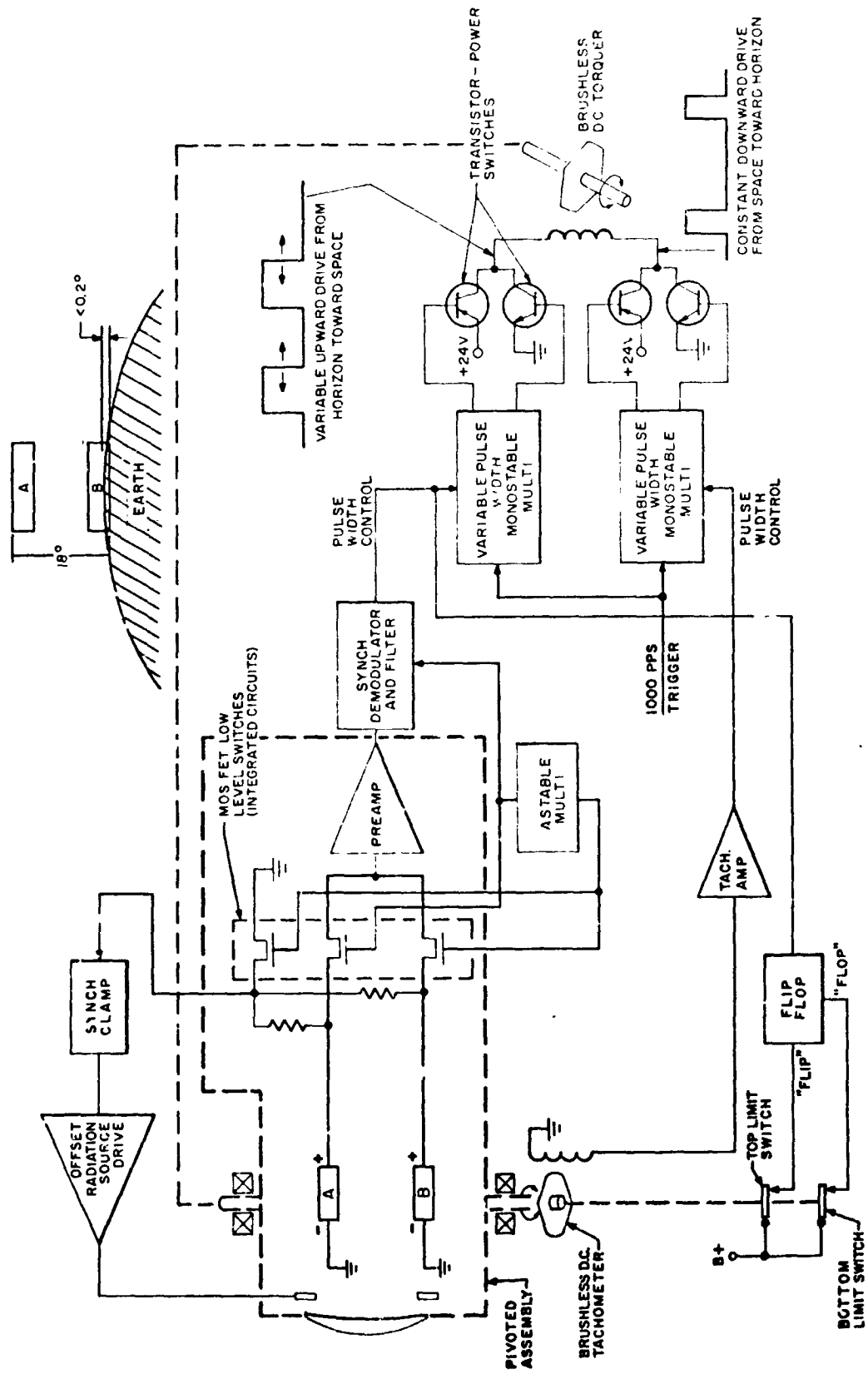


Figure 1
 CROSS SECTION OF THERMOPILE HORIZON EDGE TRACKER

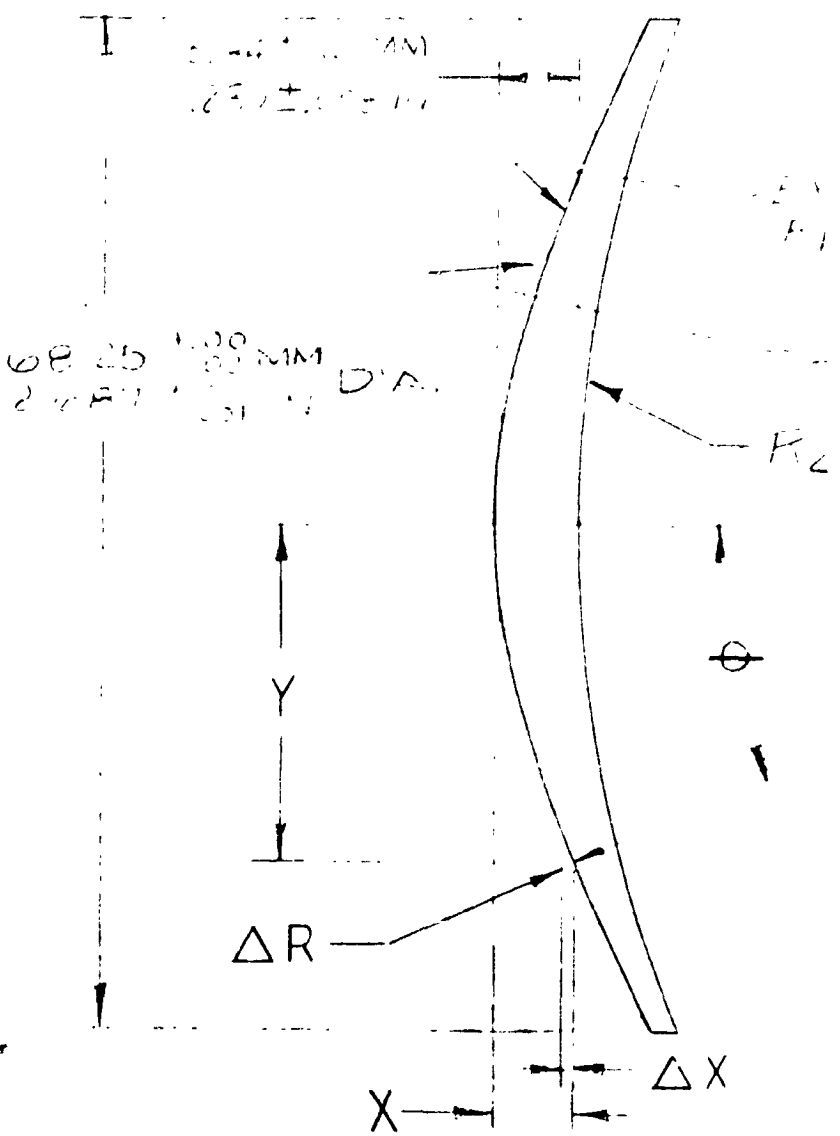


21905

Figure 2 BLOCK DIAGRAM OF ONE HEAD THERMOPILE HORIZON EDGE TRACKER

FOLDOUT FRAME FOLDOUT FRAME

RADIUS	TOL	CC	CX	SURFACE CODE	REGTY TCL OVER CA IN FRINGES	COATING			CLEAR APERTURE
						TYPE	THK	λ IN μ	
R ₁	MM IN					SEE NOTES 4-6			MM IN
R ₂	MM IN	✓				SEE NOTES 4-6			MM IN



NOTES:
 1. Surface R₁ is aspheric with the following equation: $X = \sqrt{1 + \sqrt{1 - \frac{Y^2}{R_1^2}}}$
 $\Delta X = X - \sqrt{1 + \frac{Y^2}{R_1^2}}$
 2. See sheet 2 for Polar (C.P.)

			UNLESS OTHERWISE SPECIFIED:	
			DIMENSIONS ARE IN MILLIMETERS	DRAWN
			WEDGE TOLERANCE .03 TIR	CHECKED
			ELEMENT TO BE IN ACCORDANCE WITH MIL-0-13830	APPD
			.13 MM x 45° MINIMUM BEVELS ON ALL CORNERS AND EDGES	ISSUED
1			MATERIAL	BEC A
QTY	NEXT ASSY	USED ON	SILICON	
APPLICATION			GRADE	SPEC NO.
			OPTICAL	OTHER

EXCEPT AS MAY BE OTHERWISE PROVIDED BY CONTRACT, THESE DRAWINGS AND SPECIFICATIONS ARE THE PROPERTY OF BARNES ENGINEERING COMPANY, ARE ISSUED IN STRICT CONFIDENCE, AND SHALL NOT BE REPRODUCED, OR COPIED, OR USED AS THE BASIS FOR THE MANUFACTURE OR SALE OF APPARATUS WITHOUT PERMISSION.



9-10-66

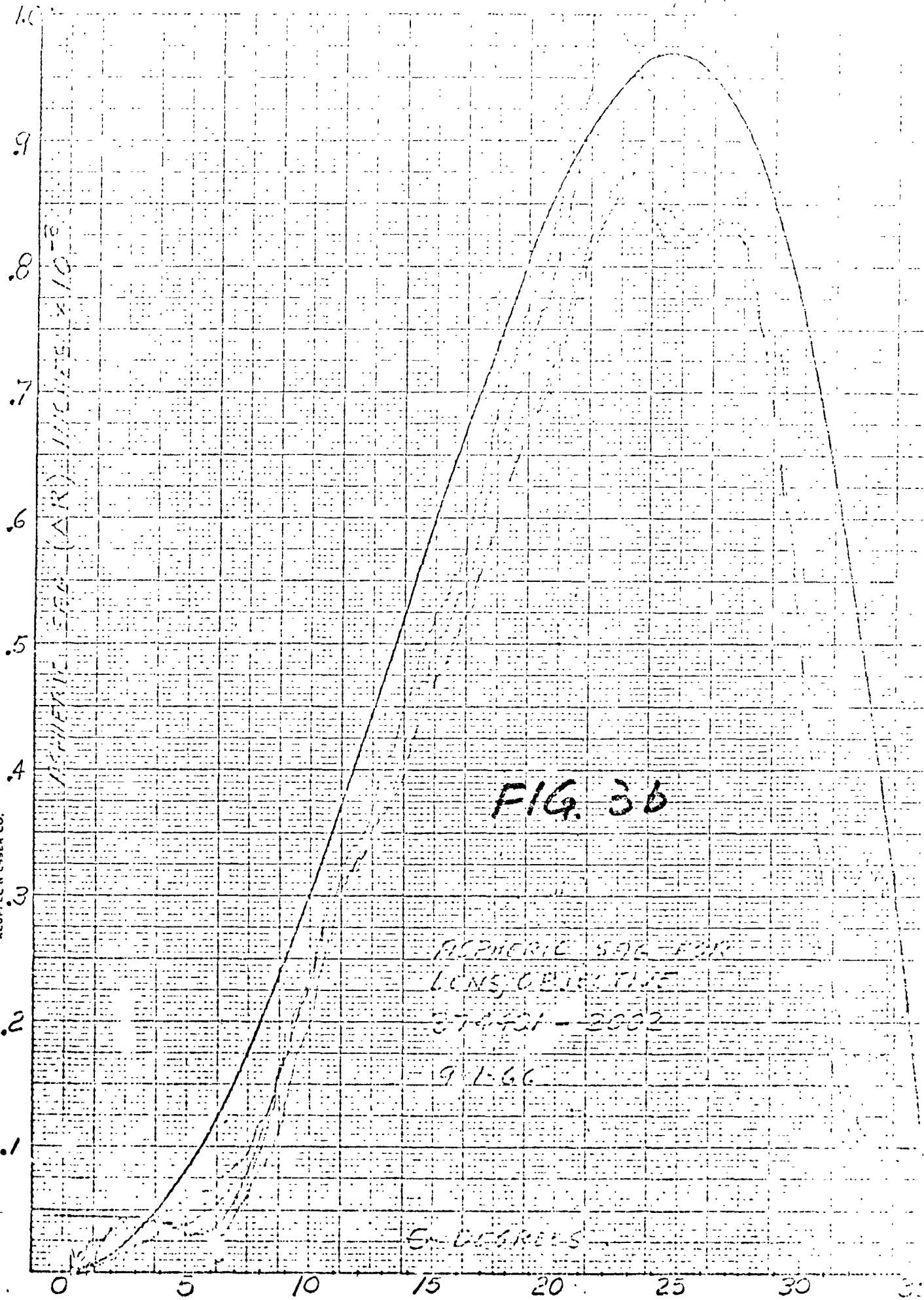


FIG. 3b

MICHELIC 596 FOR
 LENS OBJECTIVE
 STATION - 3002
 9-1-66

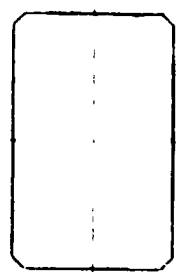
10 X TO 1/2 INCH
 46 1476
 KEUFFEL & ESSER CO.
 MADE IN U.S.A.

FOLDOUT FRAME

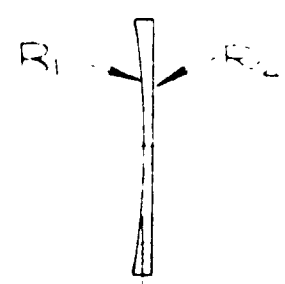


	RADIUS	TOL	CC	CX	SURFACE CODE	IRREGTY TOL OVER CA IN FRINGES	COATING			CLEAR APERTURE
							TYPE	THK	λ IN μ	
R ₁	105.59 MM	± 1.02	✓		80-20	20	SEE NOTE	1		
	4.157 IN.	$\pm .040$								
R ₂	∞ MM	$\pm 30\%r$	-	-	50-20	± 30	SEE NOTE	1		
	∞ IN.	$\pm 30\%r$								

1.52 \pm .25 MM
 .06 \pm .01 IN CHAMFER (TYP)



34.54 \pm .02 MM
 1.360 \pm .001 IN



22.23 \pm .005 MM
 .875 \pm .001 IN

1.02 \pm .10 MM
 .040 \pm .004 IN

REF: OPTICAL

			UNLESS OTHERWISE SPECIFIED:	
			DIMENSIONS ARE IN MILLIMETERS	DRAW
			WEDGE TOLERANCE .04 TIR	CHEC
			ELEMENT TO BE IN ACCORDANCE WITH MIL-0-13830	APPD
1			.25 MM X 45° MINIMUM BEVELS ON ALL CORNERS AND EDGES	ISSU
QTY	NEXT ASSY	USED ON	MATERIAL	
APPLICATION			SILICON	BEC
			GRADE OPTICAL	OTH
			SPEC NO.	

EXCEPT AS MAY BE OTHERWISE PROVIDED BY CONTRACT, THESE DRAWINGS AND SPECIFICATIONS ARE THE PROPERTY OF BARNES ENGINEERING COMPANY, ARE ISSUED IN STRICT CONFIDENCE, AND SHALL NOT BE REPRODUCED, OR COPIED, OR USED AS THE BASIS FOR THE MANUFACTURE OR SALE OF APPARATUS WITHOUT PERMISSION.



FOLD: 2

CLEAR APERTURE	REVISIONS			
	SYM	DESCRIPTION	DATE	APPROVED
MM				
IN				
MM				
IN				

374401-2003


NOTES:

1. 14 MICRON CUT ON FILTER TO BE APPLIED TO SURFACES R₁ AND R₂ SEE SHEETS 2 & 3
2. CLEAR APERTURE OF SURFACES R₁ AND R₂ TO BE INSIDE .8mm (.032 IN.) ANNULUS.

1.10 MM
.04 IN

OCT 25 1966

TITLE DATA SHEET A374401-2004 SHEETS 1 & 2

APPROVED:	SIGNATURE		DATE	 BARNES ENGINEERING COMPANY STAMFORD, CONNECTICUT LENS, FIELD FLATTENING FIG. 3c
DESIGNERS	DRAWN	<i>[Signature]</i>	4-20-66	
TITLE	CHECKED	<i>[Signature]</i>	5-12-66	
APPROVAL	APPD	<i>[Signature]</i>	5-12-66	
	APPD	<i>[Signature]</i>	5-12-66	
LEVELS	ISSUED			
BEC APPROVAL		CODE IDENT NO.	DWG	
OTHER APPROVAL		00430	B	
		SCALE 1/1	SIZE	
			374401-2003	
			SHEET 1 OF 3	

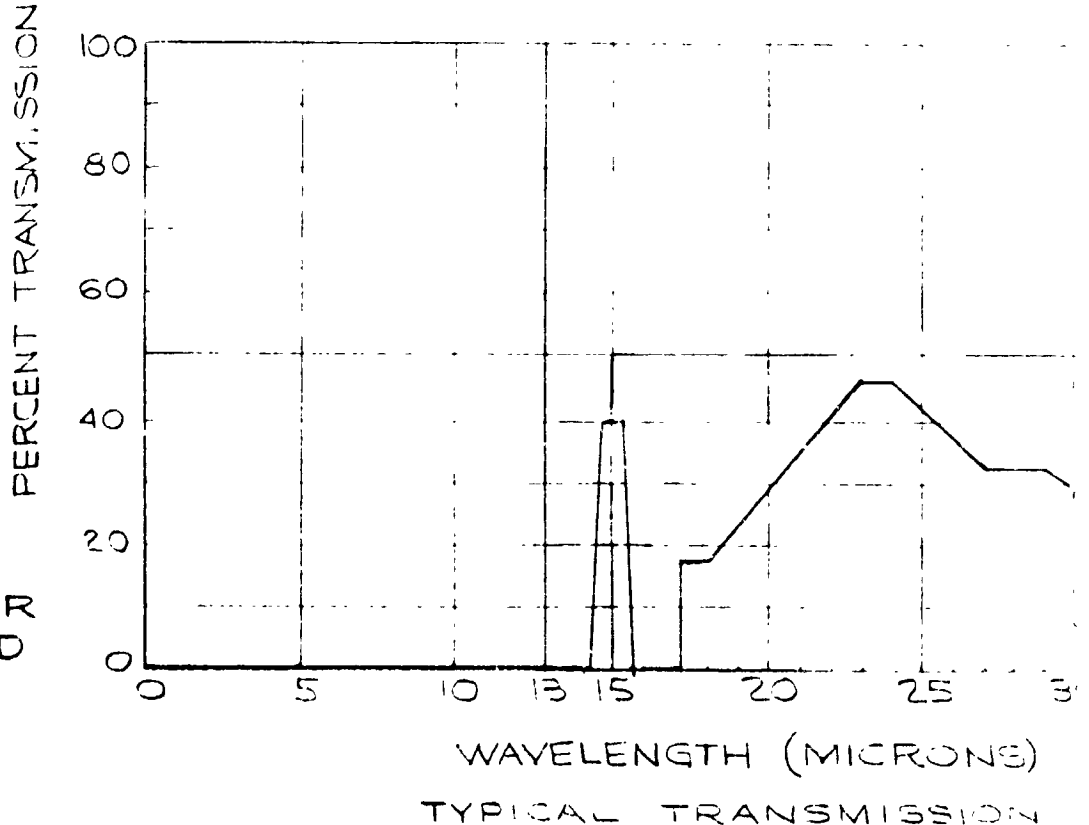
FOLDOUT

RADIUS	TOL	CC	CX	SURFACE CODE	IRREGTY TOL OVER CA IN FRINGES	COATING			CLEAR APERTURE
						TYPE	THK	λ IN μ	
R ₁	MM								
	IN								
R ₂	MM								
	IN								

WEIGHTED AVERAGE TRANSMISSION = $\sum \bar{T} \Delta \lambda M \Delta \lambda$
 TO BE 0.3 MAXIMUM FROM 0 TO 13 μ

λ	T AVG.
14.5 μ - 15.5 μ	40%
17 μ - 18 μ	18%
23 μ - 24 μ	46%
27 μ - 29 μ	33%
34 μ - 35 μ	17%

$\Delta \lambda$	M $\Delta \lambda$
0-5	27.4
5-1	45.5
1-2	20.7
2-3	3.57
3-4	1.04
4-5	.406
5-6	.189
6-7	.100
7-8	.058
8-9	.036
9-10	.023
10-11	.016
11-12	.011
12-13	.006



$\bar{T} \Delta \lambda$ = INTEGRATED TRANSMISSION OVER WAVELENGTH BAND $\Delta \lambda$ (PERCENT)

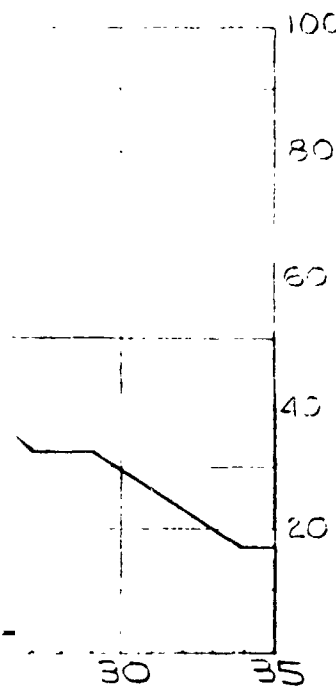
			UNLESS OTHERWISE SPECIFIED:	
			DIMENSIONS ARE IN MILLIMETERS	DRAW
			WEDGE TOLERANCE	CHEC
			ELEMENT TO BE IN ACCORDANCE WITH MIL-O-13830	APPD
1			MM x 45° MINIMUM BEVELS ON ALL CORNERS AND EDGES	ISSUE
QTY	NEXT ASSY	USED ON	MATERIAL	BEC
APPLICATION				
EXCEPT AS MAY BE OTHERWISE PROVIDED BY CONTRACT, THESE DRAWINGS AND SPECIFICATIONS ARE THE PROPERTY OF BARNES ENGINEERING COMPANY, ARE ISSUED IN STRICT CONFIDENCE, AND SHALL NOT BE REPRODUCED, OR COPIED, OR USED AS THE BASIS FOR THE MANUFACTURE OR SALE OF APPARATUS WITHOUT PERMISSION.			GRADE	OTR
			SPEC NO.	

FOLDOUT FRAME

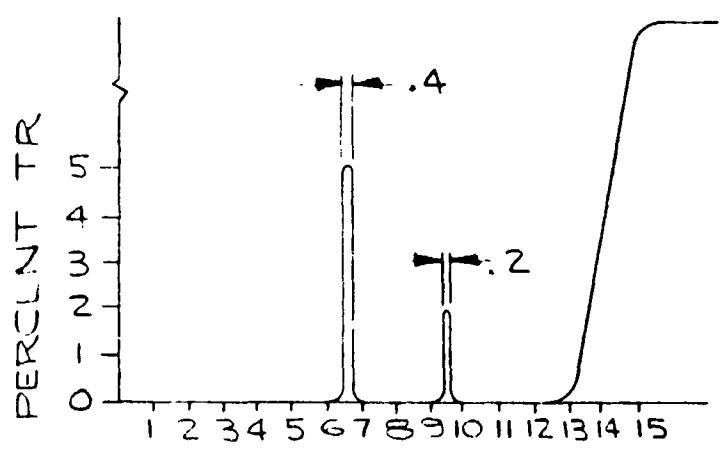
REVISIONS		DATE	APPROVED
SYM	DESCRIPTION		
	SEE SHEET 1		

LEARN
PURTURE

MM
IN
MM
IN



EXAMPLE



$$\Sigma \bar{T} \Delta \lambda M \Delta \lambda = 5 \times \left(\frac{.4}{1}\right) \times .100 + 2 \times \left(\frac{.2}{1}\right) \times .023$$

$$= .200 + .009 = .209 < .3$$

(ACCEPTABLE)

(S)
ON CURVE

OCT 25 1966

	SIGNATURE	DATE
S	<i>[Signature]</i>	5/12/66
	<i>[Signature]</i>	5/11/66
	<i>[Signature]</i>	5/12/66
S		

B E BARNES ENGINEERING COMPANY
STAMFORD, CONNECTICUT

LENS, FIELD FLATTENING
FIG. 3d

BEC APPROVAL
OTHER APPROVAL

CODE IDENT NO. 00430	DWG B	SIZE 374401-2003
SCALE	SHEET 2 OF 3	

Figure 4
HORIZON PROFILES

14-35 MICRON RANGE

- A. ARDC STANDARD - CLEAR
- B. TEMPERATE - SUMMER - CLEAR
- C. TROPICAL - SUMMER - OVERCAST
- D. ARCTIC - WINTER - OVERCAST

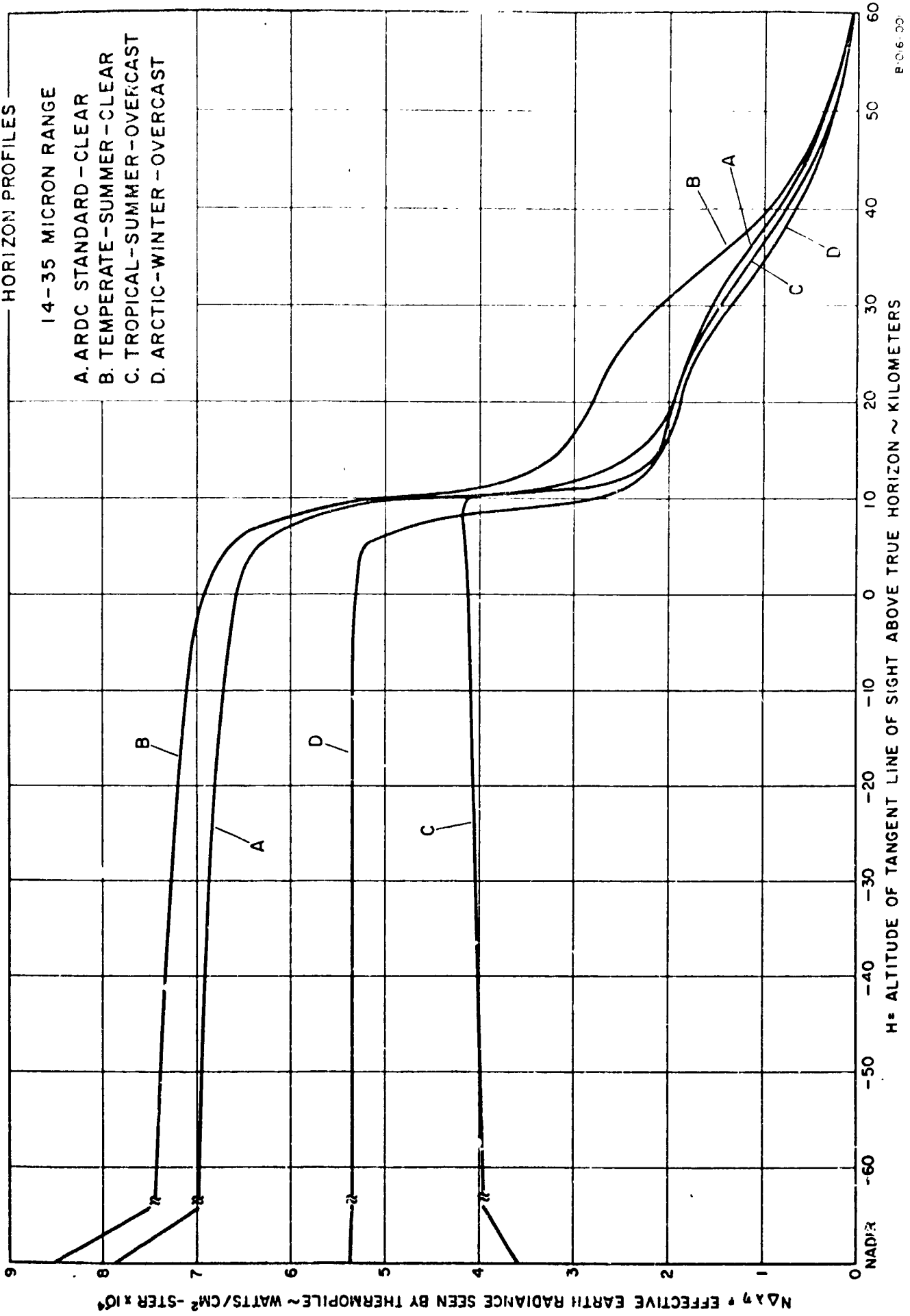
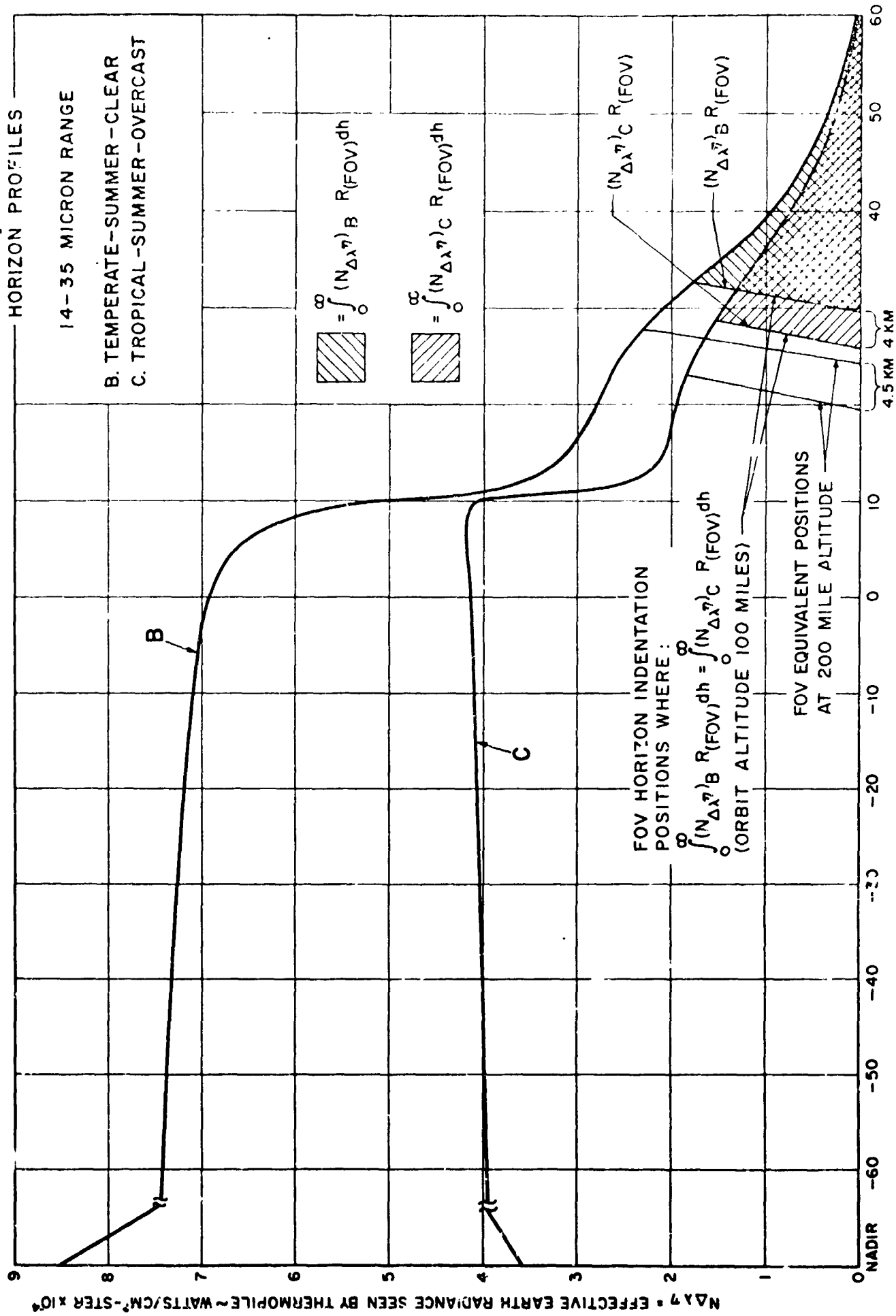


Figure 5



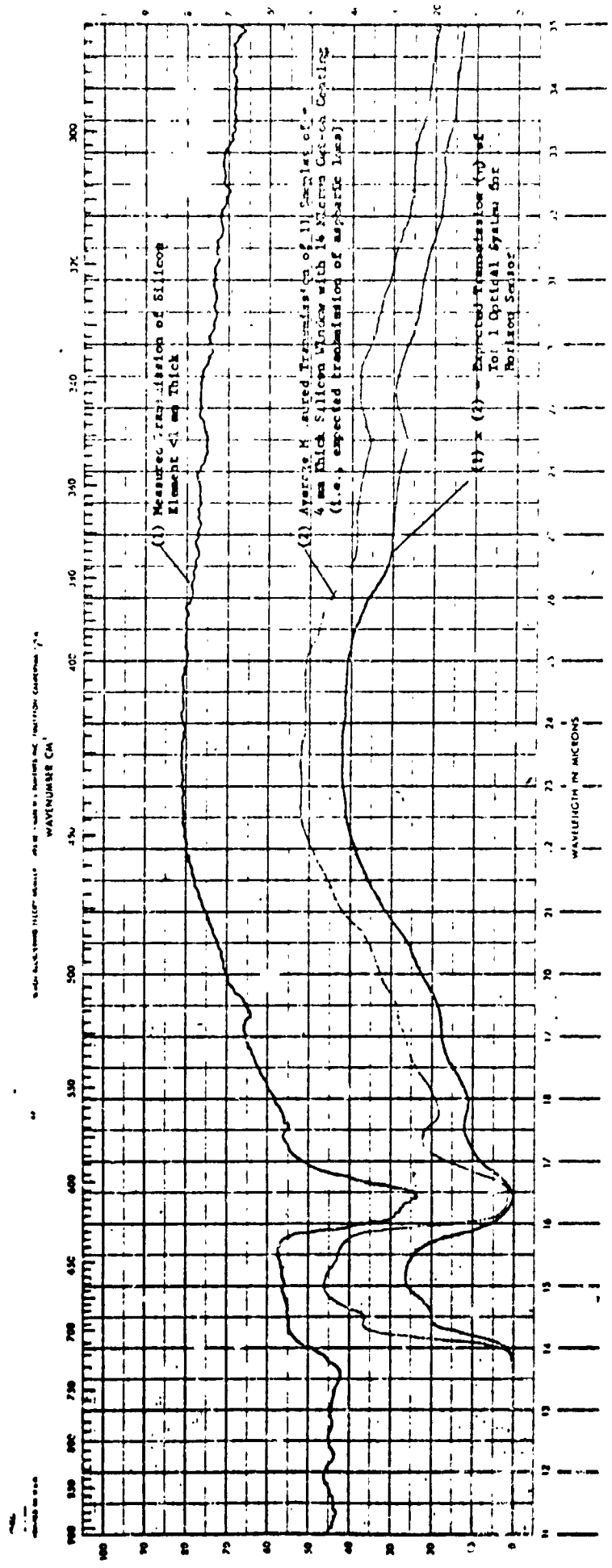
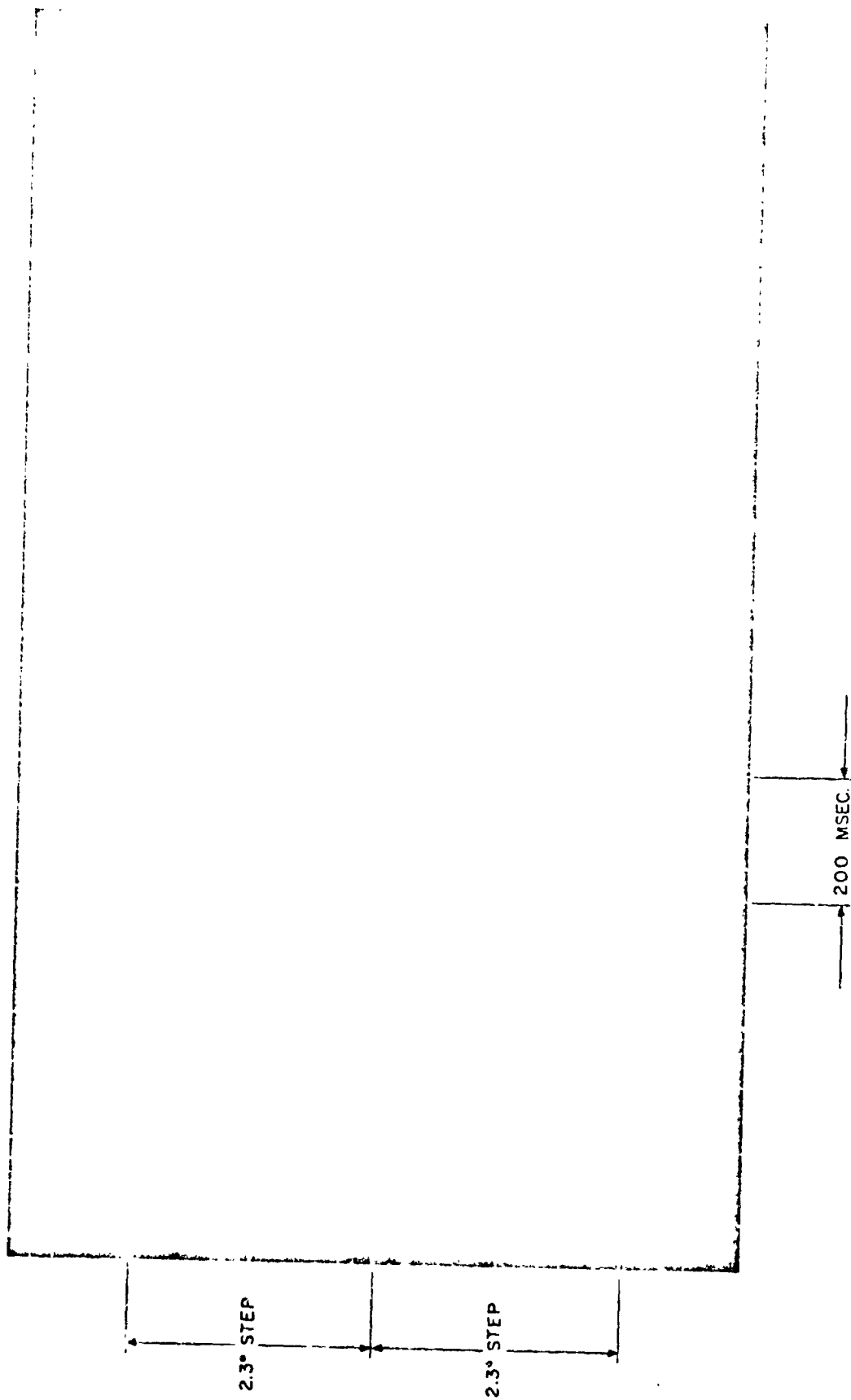


FIGURE 6 Spectral Transmission of Sensor Optics



AICIC-004

Figure 7 TIME RESPONSE FOR TRANSIENT ATTITUDE CHANGE

C-2

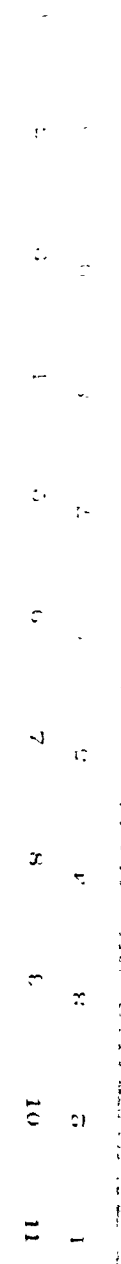
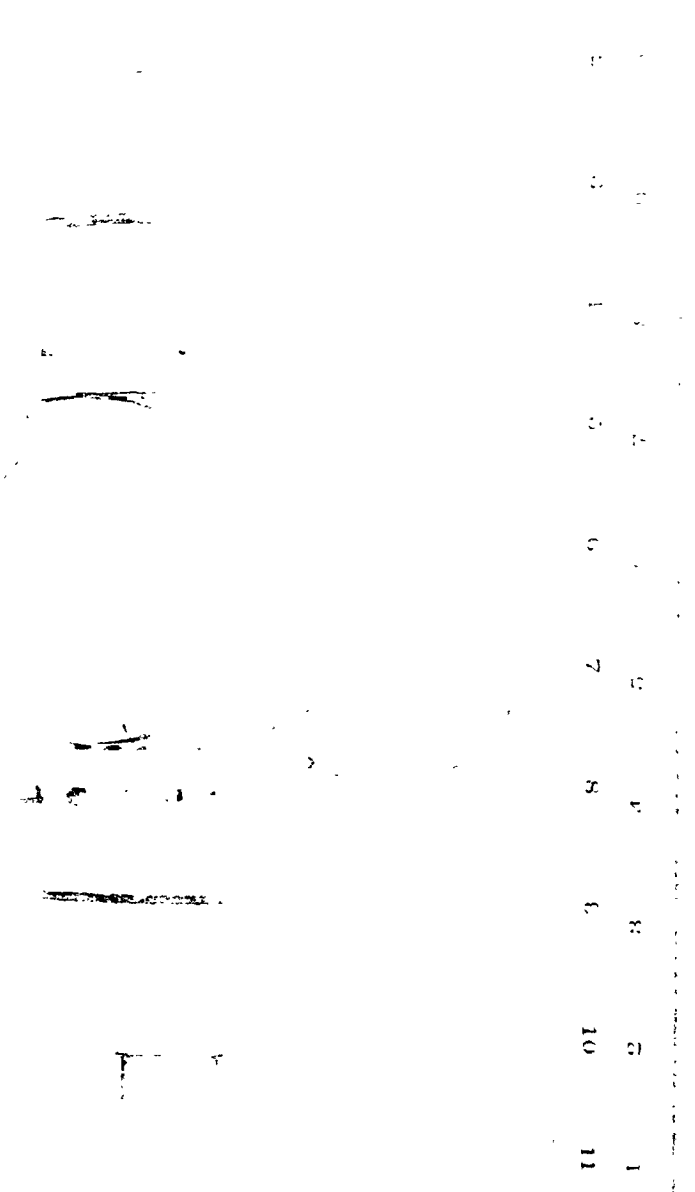
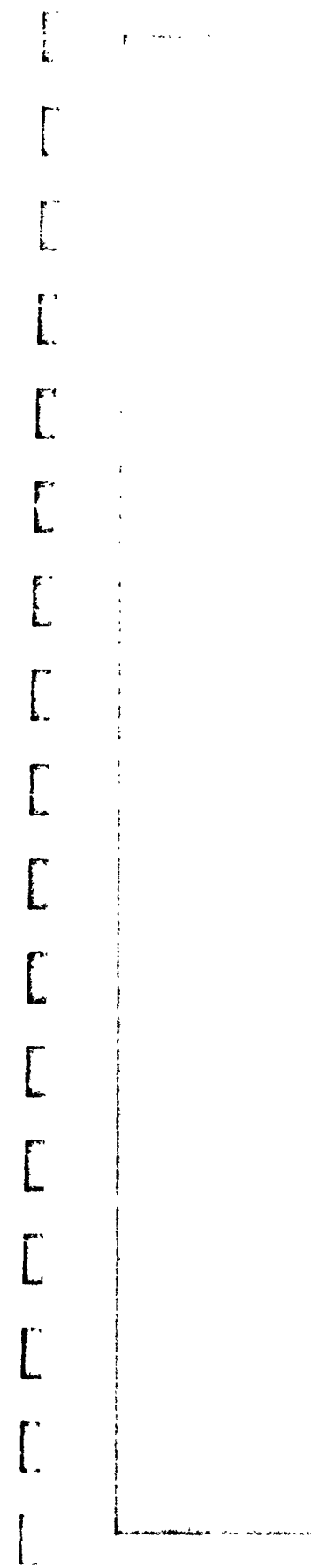


Figure 8 THERMOPILE EDGE TRACKER